Dynamics of Topological Polarization Singularity in Momentum Space

Yixuan Zeng,[1,2] Guangwei Hu,[2,*] Kaipeng Liu,[2] Zhixiang Tang,[1,†] and Cheng-Wei Qiu[2,3,‡]
[1]College of Computer Science and Electronic Engineering, Hunan University, Changsha 410082, China
[2]Department of Electrical and Computer Engineering, National University of Singapore, Singapore 117583, Singapore
[3]National University of Singapore Suzhou Research Institute, Suzhou 215125, China

(Received 27 April 2021; accepted 21 September 2021; published 22 October 2021)

The polarization singularity in momentum space has recently been discovered as a new class of topological signatures of Bloch modes in photonic crystal slabs concerning the far-field radiations, beyond its near-field description with widely explored topological band theory. Bound states in the continuum (BICs) in photonic crystal slabs are demonstrated as vortex eigenpolarization singularities in momentum space and the circular polarization points (C points) are also obtained based on BICs, opening up more possibilities for exotic light scattering and various topological phenomena of singular optics. Here, focusing on the nondegenerate bands, we report the generation to annihilation of two pairs of C points in momentum space in the photonic crystal slabs with inversion symmetry but broken up-down mirror symmetry. Interestingly, as the C points evolve with the structure parameter, we find two merging processes of C points, where an accidental at-Γ BIC and unidirectional radiative resonances with leaky channels of drastically different radiative lifetime emerge. The whole evolution is governed by the global charge conservation and the sum of topological charges equals to zero. Our findings suggest a novel recipe for dynamic generation and manipulation of various polarization singularities in momentum space and might shed new light to control the resonant and topological properties of light-matter interactions.

DOI: 10.1103/PhysRevLett.127.176101

Polarization is one of the most fundamental properties of electromagnetic radiations due to its transverse wave nature. For a monochromatic vectorial electromagnetic field, its polarization is generally position dependent, and the field can manifest complex spatial polarization patterns. One remarkable feature in the overall spatial patterns is the topological polarization singularity including C points (circular polarization points), L lines (a curve along which the polarization is linear), and V points (the vortex center of polarization fields) [1–9]. Both C points and L lines are topologically robust and generic in the polarization field, promising for controlling the directionality [10,11] and intrinsic properties [12] of quantum dot emissions, while V points, as the unstable and nongeneric singular points, also have potential applications such as subwavelength focusing [13], imaging [14], and trapping [15].

Analogous to polarization vector distributions in real space, the singular points of polarization can exist in momentum space [16–23], characterized by the far-field polarization distribution of eigenmodes in an optical system. For instance, photonic crystal slabs (PCSs) can support V points of polarization vector fields in the momentum space, which is closely related to bound states in the continuum (BICs) [19–23]. BICs are resonances with infinite lifetimes although they appear within the continuous leaky radiation spectrum [24–27]. Since far-field polarizations of eigenmodes at V points are ill-defined, the radiation loss will vanish at the corresponding specific momentum points, forming the so-called BICs with infinite radiative quality factors (Q factor) and significantly enhanced light-matter interactions [28–32]. Such V points in momentum space, which are usually characterized by an integer topological charge, open many new applications in the creation of optical vortex [33,34] and ultrahigh-Q guided resonances [35,36].

Different from V points that carry integer topological charges, C points, a more generic form of polarization singularity, have half-charge and can also exist in the far-field polarization vector fields of PCSs [37–45]. The eigenmodes at C points have finite Q factors and only couple to circularly polarized radiative waves, which are directly associated with chiroptical effects [46,47] and facilitate intriguing applications like routing the valley exciton emission [48]. Recently, C points are observed near the band degeneracies and are shown to be related with the nontrivial Berry phase of bands [42–45]. For the nondegenerate bands with trivial Berry phase, the generation and manipulation of half-charged C points are usually associated with the V points in the up-down mirror symmetric PCSs, i.e., BICs [37–41]. For example, pairwise C points can be created by breaking the symmetry-protected BICs in PCSs [37–39]; merging two C points, originally separated from an off-Γ BIC (V point), of downward radiations can generate unidirectional guided resonances (UGRs) that only radiate to the upward direction [40]. However, for various practical applications

enabled by C points in momentum space, more abundant and flexible mechanisms to generate and tune C points should be devised.

In this study, we propose a general and simple approach of two misaligned stacked dielectric gratings, which shows a complete evolution process of C points starting from *zero* topological charge, including the generation, merging, and annihilation. Distinct from the fact that the C points generated from BICs by breaking the in-plane C_2 symmetry have identical charges and opposite handedness [37–41], two pairs of C points, each of which possesses the same handedness but opposite topological charges, can be created and dynamically manipulated via continuously shifting of the misalignment without breaking the inversion symmetry of structure. Besides, two merging processes of half-charged C points with the same topological charges but different handedness into accidental V points are observed for the first time. Importantly, owing to the broken up-down mirror symmetry and the preserved inversion symmetry of the structure, the high-contrast directional radiations and accidental perfect BICs are achieved at these accidental V points. These distinguished topological polarization evolutions are closely related to the symmetry of our system, which are also bounded by the conservation of global topological charge. It is worth noting that the total topological charges are strictly zero during the whole process.

Here, the one-dimensional PCSs [49–51] composed by two superimposed identical high refractive index gratings ($n_1 = 3.48$) with lattice constant a, width $w = 0.461a$, and slab thickness $h = 0.32a$, in the background medium of low refractive index ($n_2 = 1.46$), is shown in Fig. 1(a). In general, such PCSs has broken mirror symmetry with respect to x-y plane (σ_z symmetry), when the lateral offset or misalignment δ exists, but preserves the inversion symmetry (P symmetry). At the highly symmetric case when $\delta = 0$, the transverse electric (TE) band structure, which describes the Bloch modes in PCSs, along the k_x axis is obtained by finite-element simulation methods and plotted in Fig. 1(b). The modes at the Γ point for the first (TE_1) and second (TE_2) bands are symmetry-protected BICs that carry integer topological charges and to exclude the influences of them, the following studies focus on the third band (TE_3). Figure 1(c) depicts the electric field distribution of TE_3 mode at Γ point, indicating the existence of leaky waves. When the misalignment δ is introduced and varies, a variety of topological polarization singularities can be generated and fully manipulated by this misalignment.

To start, we first quantitatively discuss the topological charge q of polarization singularity supported by PCSs in momentum space. For a nondegenerate Bloch mode with an in-plane wave vector $\boldsymbol{k}_\parallel = (k_x, k_y)$ above the light line and below the diffraction limit, the only propagating wave compatible with it is the zero-order Fourier component of

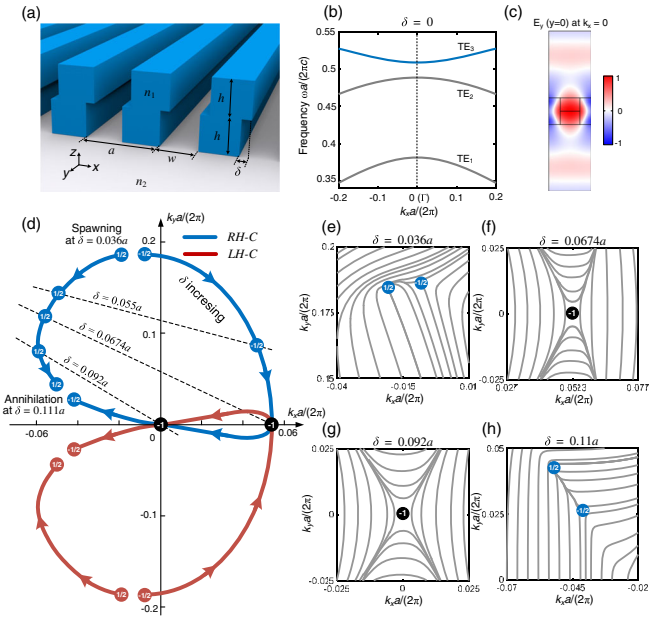

FIG. 1. The evolution of polarization singularities in momentum space supported by one-dimensional photonic crystal slab. (a) Schematics of a one-dimensional photonic crystal slab composed of two superimposed identical gratings with a misalignment δ. (b) Calculated TE band structure along the k_x axis at $\delta = 0$. The blue line is the third TE band (TE_3) that we focus on. (c) Mode profile in the unit cell for the TE_3 band at Γ point. (d) Trajectories traced by two pairs of C points with different topological charges ($q = \pm 1/2$) in momentum space as δ increases for downward radiation. The blue and red discs marked by $\pm 1/2$ indicate the right-handed and left-handed circular polarizations with a topological charge of $\pm 1/2$. (e)–(h) show the calculated projected polarization vector fields of downward radiation when $\delta = 0.036a$ (e), $0.0674a$ (f), $0.092a$ (g), $0.1a$ (h). The black discs are the V points with charge $q = -1$.

Bloch functions and has the same $\boldsymbol{k}_\parallel$ [19,24]. To investigate the topology in $\boldsymbol{k}_\parallel$ space, a polarization vector of far-field radiation projected onto x-y plane is introduced, $\boldsymbol{d}(\boldsymbol{k}_\parallel) = d_x(\boldsymbol{k}_\parallel)\hat{x} + d_y(\boldsymbol{k}_\parallel)\hat{y}$. The topological charge q carried by the polarization singularity for $\boldsymbol{d}(\boldsymbol{k}_\parallel)$ is thus defined as [19,38]:

$$q = \frac{1}{2\pi}\oint_L d\boldsymbol{k}_\parallel \cdot \nabla_{\boldsymbol{k}_\parallel}\phi(\boldsymbol{k}_\parallel), \tag{1}$$

where L is a closed path in the $\boldsymbol{k}_\parallel$ space that goes around the polarization singularity in the counterclockwise direction. $\phi(\boldsymbol{k}_\parallel) = \frac{1}{2}\arg[S_1(\boldsymbol{k}_\parallel) + iS_2(\boldsymbol{k}_\parallel)]$ is the angle between its long axis of the polarization ellipse and the x axis, and $S_i(\boldsymbol{k}_\parallel)$ is the Stokes parameter of $\boldsymbol{d}(\boldsymbol{k}_\parallel)$ (Supplemental Material [52], Sec. S1). Topological charge q describes how many times the polarization vector winds along a closed loop L and has a similar form to the Chern number defined in bulk bands. Once the polarization vector cannot

be continuously defined, nonzero topological charges necessarily emerge, generating polarization singularities in momentum space. The charge q is half-integer if the loop L encloses a C point where $S_1 = S_2 = 0$ and $S_3 = \pm 1$ [37,38], while q is an integer if a V point is enclosed where $S_1 = S_2 = S_3 = 0$ (i.e., the vanished radiation intensity) [17–23]. Generally, V points represent BICs in the system with σ_z symmetry, since, at this point, no radiation channels are allowed though the mode exists within the light cone [19–25].

We now show the generation and evolution of various topological polarization singularities in our system, which is also discussed in Sec. S2 of Supplemental Material [52] by utilizing the temporal coupled-mode theory [57–59]. Since our system preserves P symmetry, the projected polarization vector distribution in downward radiation ($k_z < 0$) is inverse to that in upward radiation ($k_z > 0$) (Supplemental Material [52], Sec. S2). Thus, we can study the half-space radiation to understand our system. Figure 1(d) shows the evolution of C points in momentum space with different misalignments for downward radiations. The right-handed and left-handed C points, dubbed RH-C and LH-C points respectively, are marked as blue and red lines. At $\delta = 0.036a$, a pair of RH-C points emerge in the vicinity of $\boldsymbol{k}_\parallel a/(2\pi) = (-0.015, 0.185)$. They have opposite topological charges ($q = \pm 1/2$) and can be further seen from projected polarization vector distribution in Fig. 1(e), which is represented by the line field tangent to the long axis of the polarization ellipse. We can explicitly observe the "star" and "lemon" patterns, further verifying the existences of C points with $-1/2$ and $1/2$ charges [4]. Since the topological charge is a conserved quantity, it will only deform and move in momentum space but cannot suddenly appear or disappear due to the topological robustness. Therefore, for C points, the destruction and generation are only possible pairwise: a C point can only be removed through collision with another C point of same handedness but opposite charge [37–42], which accounts for our observed generation of paired C points with opposite topological charges. Moreover, bounded by y-mirror symmetry (σ_y symmetry), another pair of LH-C points necessarily appear near $\boldsymbol{k}_\parallel a/(2\pi) = (-0.015, -0.185)$ (Supplemental Material [52], Sec. S2). Importantly, our discovered C points are generated from zero topological charge, distinct from recently reported C points by breaking an integer-charged V point [37–41], which points out the fundamental nature and general existence of C points in momentum space.

More interestingly, as the misalignment δ increases, these C points can be dynamically tuned and can collapse in momentum space. At $\delta = 0.0674a$, as seen in Fig. 1(d), two C points with opposite handedness and identical charge $q = -1/2$ merge at k_x axis, $\boldsymbol{k}_\parallel a/(2\pi) = (0.0523, 0)$, becoming a V point. Figure 1(f) displays the polarization line field of downward radiation at $\delta = 0.0674a$, where the V point is marked as the black disc. As mentioned, due to the preserved P symmetry, the polarization state distribution of upward radiation is inverse to that of downward radiation and the V point in upward radiation will appear at $\boldsymbol{k}_\parallel a/(2\pi) = (-0.0523, 0)$. For better understanding, we calculate the far-field polarization states in upward and downward radiation when $\delta = 0.0674a$ and plot them in Fig. 2(a), which obviously suggest the inversion relationship between the polarization state distribution of upward (top panel) and downward (bottom panel) radiation. Because the far-field polarization at V points is ill-defined, the radiation intensity would vanish [19,40] and two UGRs, which have different radiative channels, are achieved. Such UGRs are characterized with drastically different radiative lifetimes for upward and downward radiations, presenting the unidirectional radiation feature due to the broken σ_z symmetry (Supplemental Material [52], Sec. S2). To verify the UGRs, we calculate the radiative losses toward the top (γ_u) and bottom (γ_d) of the structure and get an asymmetry ratio, $\eta = \gamma_u/\gamma_d$, for different $\boldsymbol{k}_\parallel$ point. Figure 2(b) depicts that the upward (orange) and downward (dashed green) radiation losses are almost reduced to 0 at $\boldsymbol{k}_\parallel a/(2\pi) = (-0.0523, 0)$ and $\boldsymbol{k}_\parallel a/(2\pi) = (0.0523, 0)$, respectively, i.e., the position of the two UGRs. They are also consistent with the extremely bright spots in Fig. 2(c), which exhibits the asymmetry ratio η in momentum space.

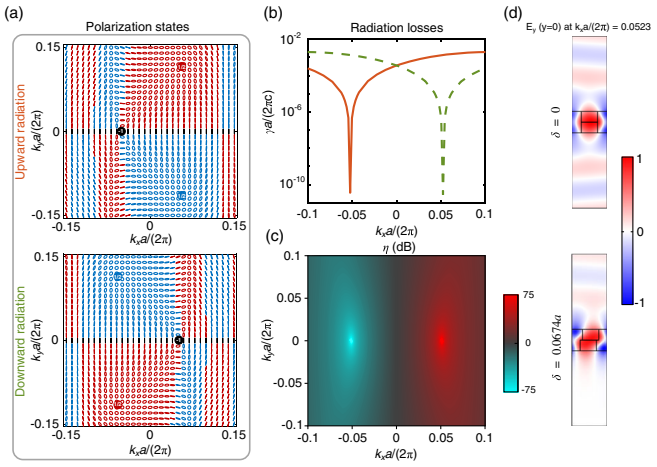

FIG. 2. The far-field polarization states, radiation losses, asymmetry ratio, and electric field profiles of eigenmodes. (a) Far-field polarization states in upward and downward radiation in momentum space for $\delta = 0.0674a$. The blue (red) ellipse denotes the right (left)-handed elliptic polarizations with different major axes orientation. The black lines on the k_x axis represent the linear y polarization. (b) Radiation losses from eigenmodes along the k_x axis toward the top γ_u (orange) and bottom γ_d (dashed green) of the structure with $\delta = 0.0674a$. (c) The asymmetry ratio between upward and downward radiative loss, $\eta = \gamma_u/\gamma_d$, for $\delta = 0.0674a$. (d) Electric field profiles (y component) of the eigenmodes at $\boldsymbol{k}_\parallel a/(2\pi) = (0.0523, 0)$ for $\delta = 0$ (top panel) and $\delta = 0.0674a$ (bottom panel).

In addition, from the electric field profiles (y component) at $\boldsymbol{k}_{\parallel}a/(2\pi) = (0.0523, 0)$ for $\delta = 0$ and $\delta = 0.0674a$ shown in Fig. 2(d), we can clearly observe that the UGR only radiates upward. The coexistence of these two UGRs at the obtained V points shows that the radiative channels can be controlled by the in-plane propagation direction of lights and could be utilized to increase the efficiencies of diverse optical devices, such as vertical emitting lasers and grating couplers.

Further increasing δ leads to the splitting of V points. As plotted in Fig. 1(d), when δ increases from $0.0674a$ to $0.092a$, two C points with same charge $q = -1/2$ are spawned from the V point and moving toward the Γ point, i.e., $\boldsymbol{k}_{\parallel}a/(2\pi) = (0, 0)$. At $\delta = 0.092a$, they cross into each other and act as a V point again at Γ point, which is labeled in Fig. 1(g). Because the Γ point in momentum space is a high symmetric point, the negative half-charged C points in upward radiation as well remerge into a V point at Γ point for $\delta = 0.092a$. Figures 3(a)–3(c) show the far-field polarization states in upward radiation when $\delta = 0.0674a$, $0.08a$, and $0.092a$, respectively, while the counterparts in downward radiation are shown in Figs. 3(d)–3(f). Owing to the vanished radiation intensities in both upward and downward leaky channels, the state at Γ point becomes a perfect BIC, not radiating either upward or downward (Supplemental Material [52], Sec. S2). To prove the nonradiative feature of this BIC, we also calculate the radiative losses γ_u and γ_d along the k_x axis and the Q factor in momentum space for $\delta = 0.092a$ [Figs. 4(a) and 4(b)]. We observe that, at Γ point, γ_u and γ_d both reduce to 0 and the Q factor diverges. Furthermore, the modal electric field profile at the Γ point also shows that there are no outgoing waves from the mode [Fig. 4(c)]. These results unambiguously verify the emergence of BIC, not quasi-BIC [60], by manipulating the C points in momentum space. It is worth noting that, although this BIC is at the Γ point, it is an accidental BIC, which is distinct from the at-Γ BICs protected by the in-plane rotation symmetry in σ_z symmetric PCSs [25,27].

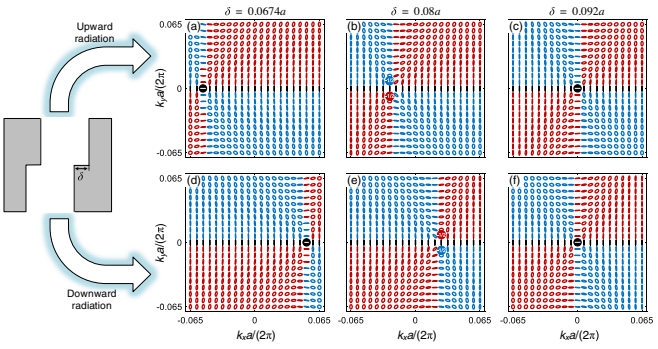

FIG. 3. Evolution of polarization singularities. (a)–(c) show far-field polarization states of eigenmodes in upward radiation of structures with increasing (a) $\delta = 0.0674a$, (b) $0.08a$, (c) $0.092a$, respectively. Far-field polarization states of eigenmodes in downward radiation corresponding to (d)–(f).

Meanwhile, as δ increases, the other two C points of charge $q = 1/2$ are also moving in momentum space following the trajectories shown in Fig. 1(d). When $\delta = 0.0674a$ and $\delta = 0.092a$, the RH-C point with charge $q = 1/2$ in downward radiation is located at $\boldsymbol{k}_{\parallel}a/(2\pi) = (-0.057, 0.116)$ and $(-0.061, 0.082)$, respectively [Figs. 2(a) and 4(d)]. The positions $\boldsymbol{k}_{\parallel}a/(2\pi)$ of the LH-C point with charge $q = 1/2$ are correspondingly equal to $(-0.057, -0.116)$ and $(-0.061, -0.082)$. Increasing δ from $0.092a$, the V point at the Γ point would be destroyed into two C points with charge $q = -1/2$ again. Then the C points with identical handedness but opposite charge move toward each other. Figure 1(h) exhibits that two RH-C points with opposite half-charge in downward radiation meet near $\boldsymbol{k}_{\parallel}a/(2\pi) = (-0.045, 0.035)$ at $\delta = 0.11a$. Finally, these two RH-C points are annihilated with each other when δ reaches $0.111a$ (for details of the evolution of C points, see Supplemental Material [52], Sec. S3). For another pair of LH-C points, the same is true. It is worth pointing out that in the whole process, the topological charges are consistently conserved, and the sum equals zero. Furthermore, the whole process can also occur in the $(\boldsymbol{k}_{\parallel}, \delta)$ space of the one-dimensional PCSs with different parameter configurations (Supplemental Material [52], Sec. S4).

While C points have been obtained by breaking the BICs with integer topological charge [37–39] and observed near non-Hermitian band degeneracies [42–45], our results show an unprecedented degree of freedom to generate and manipulate the C points in momentum space, which could be used to tailor the directionality of quantum dot emissions and valley exciton emission [48]. In addition, the

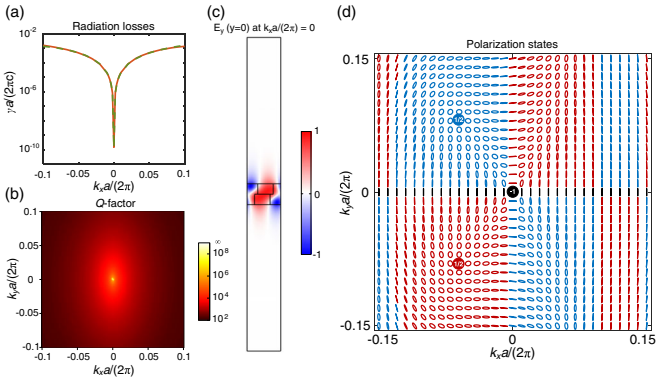

FIG. 4. The radiation losses, Q factor, electric field profile, and far-field polarization states of eigenmodes at $\delta = 0.092a$. (a) Radiation losses of eigenmodes along k_x axis toward the top γ_u (orange) and bottom γ_d (dashed green) of structures for $\delta = 0.092a$. (b) The distribution of Q factors of eigenmodes near the Γ point. (c) Electric field profiles (y component) of the accidental at-Γ BIC [$\boldsymbol{k}_{\parallel}a/(2\pi) = (0, 0)$]. (d) Far-field polarization states of eigenmodes in downward radiation.

existences of *RH-C*, *LH-C*, and linear polarization in momentum space also mean the full coverage of the Poincaré sphere, which offers a powerful capability to modulate polarization of light [61,62]. More importantly, by merging *C* points, the highly directional radiations at two URGs and the high *Q* factor at BICs are achieved here, which shows the great flexibility to obtain various polarization singularities in an on-demand manner and these remarkable features are desired in on-chip optoelectronic devices such as directional lasing [28,29], grating coupler [63,64], and other important applications [65].

In conclusion, starting from *zero* topological charge, we demonstrated a complete process, from the generation of two pairs of *C* points in the momentum space to their annihilation, in a one-dimensional PCSs with the broken σ_z symmetry but the preserved *P* symmetry. The thorough process is consistent with the sum of topological charges being equal to zero, which is distinct from the *C* points obtained from BICs. Our findings suggest a generic method for creating various polarization singularities in momentum space, such as *C* points and *V* points, that offer great flexibilities of managing the far-field radiations including their radiative channels, far-field polarization states, and quality factors of resonances, for various applications.

We acknowledge the support from the National Natural Science Foundation of China (Grants No. 61571186, No. 61731010, and No. 11874142). Y. Z. acknowledges China Scholarship Council for financial support.

*guangweihu@u.nus.edu
†tzx@hnu.edu.cn
‡chengwei.qiu@nus.edu.sg

[1] M. R. Dennis, K. O'Holleran, and M. J. Padgett, Singular optics: Optical vortices and polarization singularities, Prog. Opt. **53**, 293 (2009).
[2] K. Y. Bliokh, M. A. Alonso, and M. R. Dennis, Geometric phases in 2D and 3D polarized fields: Geometrical, dynamical, and topological aspects, Rep. Prog. Phys. **82**, 122401 (2019).
[3] M. V. Berry and M. R. Dennis, Polarization singularities in isotropic random vector waves, Proc. R. Soc. A **457**, 141 (2001).
[4] M. R. Dennis, Polarization singularities in paraxial vector fields: Morphology and statistics, Opt. Commun. **213**, 201 (2002).
[5] I. Freund, Polarization singularity indices in Gaussian laser beams, Opt. Commun. **201**, 251 (2002).
[6] M. Burresi, R. J. P. Engelen, A. Opheij, D. van Oosten, D. Mori, T. Baba, and L. Kuipers, Observation of Polarization Singularities at the Nanoscale, Phys. Rev. Lett. **102**, 033902 (2009).
[7] T. Fösel, V. Peano, and F. Marquardt, *L* lines, *C* points and Chern numbers: Understanding band structure topology using polarization fields, New J. Phys. **19**, 115013 (2017).
[8] R. W. Schoonover and T. D. Visser, Polarization singularities of focused, radially polarized fields, Opt. Express **14**, 5733 (2006).
[9] Ruchi, S. K. Pal, and P. Senthilkumaran, Generation of *V*-point polarization singularity lattices, Opt. Express **25**, 19326 (2017).
[10] B. le Feber, N. Rotenberg, and L. Kuipers, Nanophotonic control of circular dipole emission, Nat. Commun. **6**, 6695 (2015).
[11] R. J. Coles, D. M. Price, J. E. Dixon, B. Royall, E. Clarke, P. Kok, M. S. Skolnick, A. M. Fox, and M. N. Makhonin, Chirality of nanophotonic waveguide with embedded quantum emitter for unidirectional spin transfer, Nat. Commun. **7**, 11183 (2016).
[12] P. Lodahl, A. F. van Driel, I. S. Nikolaev, A. Irman, K. Overgaag, D. Vanmaekelbergh, and W. L. Vos, Controlling the dynamics of spontaneous emission from quantum dots by photonic crystals, Nature (London) **430**, 654 (2004).
[13] R. Dorn, S. Quabis, and G. Leuchs, Sharper Focus for a Radially Polarized Light Beam, Phys. Rev. Lett. **91**, 233901 (2003).
[14] C. J. R. Sheppard and A. Choudhury, Annular pupils, radial polarization, and superresolution, Appl. Opt. **43**, 4322 (2004).
[15] Q. Zhan, Trapping metallic Rayleigh particles with radial polarization, Opt. Express **12**, 3377 (2004).
[16] W. Liu, W. Liu, L. Shi, and Y. Kivshar, Topological polarization singularities in metaphotonics, Nanophotonics **10**, 1469 (2021).
[17] Y. Zhang, A. Chen, W. Liu, C. W. Hsu, B. Wang, F. Guan, X. Liu, L. Shi, L. Lu, and J. Zi, Observation of Polarization Vortices in Momentum Space, Phys. Rev. Lett. **120**, 186103 (2018).
[18] A. Chen, W. Liu, Y. Zhang, B. Wang, X. Liu, L. Shi, L. Lu, and J. Zi, Observing vortex polarization singularities at optical band degeneracies, Phys. Rev. B **99**, 180101(R) (2019).
[19] B. Zhen, C. W. Hsu, L. Lu, A. D. Stone, and M. Soljačić, Topological Nature of Optical Bound States in the Continuum, Phys. Rev. Lett. **113**, 257401 (2014).
[20] E. N. Bulgakov and D. N. Maksimov, Topological Bound States in the Continuum in Arrays of Dielectric Spheres, Phys. Rev. Lett. **118**, 267401 (2017).
[21] E. N. Bulgakov and D. N. Maksimov, Bound states in the continuum and polarization singularities in periodic arrays of dielectric rods, Phys. Rev. A **96**, 063833 (2017).
[22] H. M. Doeleman, F. Monticone, W. den Hollander, A. Alù, and A. F. Koenderink, Experimental observation of a polarization vortex at an optical bound state in the continuum, Nat. Photonics **12**, 397 (2018).
[23] W. Chen, Y. Chen, and W. Liu, Singularities and Poincaré Indices of Electromagnetic Multipoles, Phys. Rev. Lett. **122**, 153907 (2019).
[24] C. W. Hsu, B. Zhen, J. Lee, S. L. Chua, S. G. Johnson, J. D. Joannopoulos, and M. Soljačić, Observation of trapped light within the radiation continuum, Nature (London) **499**, 188 (2013).
[25] J. Lee, B. Zhen, S. L. Chua, W. Qiu, J. D. Joannopoulos, M. Soljačić, and O. Shapira, Observation and Differentiation of Unique High-*Q* Optical Resonances near Zero Wave Vector

in Macroscopic Photonic Crystal Slabs, Phys. Rev. Lett. **109**, 067401 (2012).
[26] F. Monticone and A. Alù, Embedded Photonic Eigenvalues in 3D Nanostructures, Phys. Rev. Lett. **112**, 213903 (2014).
[27] C. W. Hsu, B. Zhen, A. D. Stone, J. D. Joannopoulos, and M. Soljacic, Bound states in the continuum, Nat. Rev. Mater. **1**, 16048 (2016).
[28] A. Kodigala, T. Lepetit, Q. Gu, B. Bahari, Y. Fainman, and B. Kanté, Lasing action from photonic bound states in continuum, Nature (London) **541**, 196 (2017).
[29] S. T. Ha, Y. H. Fu, N. K. Emani, Z. Pan, R. M. Bakker, R. Paniagua-Domínguez, and A. I. Kuznetsov, Directional lasing in resonant semiconductor nanoantenna arrays, Nat. Nanotechnol. **13**, 1042 (2018).
[30] Z. Liu, Y. Xu, Y. Lin, J. Xiang, T. Feng, Q. Cao, J. Li, S. Lan, and J. Liu, High-Q Quasibound States in the Continuum for Nonlinear Metasurfaces, Phys. Rev. Lett. **123**, 253901 (2019).
[31] K. Koshelev, S. Kruk, E. Melik-Gaykazyan, J.-H. Choi, A. Bogdanov, H.-G. Park, and Y. Kivshar, Subwavelength dielectric resonators for nonlinear nanophotonics, Science **367**, 288 (2020).
[32] V. Kravtsov, E. Khestanova, F. A. Benimetskiy, T. Ivanova, A. K. Samusev, I. S. Sinev, D. Pidgayko, A. M. Mozharov, I. S. Mukhin, M. S. Lozhkin, Y. V. Kapitonov, A. S. Brichkin, V. D. Kulakovskii, I. A. Shelykh, A. I. Tartakovskii, P. M. Walker, M. S. Skolnick, D. N. Krizhanovskii, and I. V. Iorsh, Nonlinear polaritons in a monolayer semiconductor coupled to optical bound states in the continuum, Light **9**, 56 (2020).
[33] C. Huang, C. Zhang, S. Xiao, Y. Wang, Y. Fan, Y. Liu, N. Zhang, G. Qu, H. Ji, J. Han, L. Ge, Y. Kivshar, and Q. Song, Ultrafast control of vortex microlasers, Science **367**, 1018 (2020).
[34] B. Wang, W. Liu, M. Zhao, J. Wang, Y. Zhang, A. Chen, F. Guan, X. Liu, L. Shi, and J. Zi, Generating optical vortex beams by momentum-space polarization vortices centred at bound states in the continuum, Nat. Photonics **14**, 623 (2020).
[35] J. Jin, X. Yin, L. Ni, M. Soljačić, B. Zhen, and C. Peng, Topologically enabled ultrahigh-Q guided resonances robust to out-of-plane scattering, Nature (London) **574**, 501 (2019).
[36] M. Kang, S. Zhang, M. Xiao, and H. Xu, Merging Bound States in the Continuum at Off-High Symmetry Points, Phys. Rev. Lett. **126**, 117402 (2021).
[37] W. Liu, B. Wang, Y. Zhang, J. Wang, M. Zhao, F. Guan, X. Liu, L. Shi, and J. Zi, Circularly Polarized States Spawning from Bound States in the Continuum, Phys. Rev. Lett. **123**, 116104 (2019).
[38] T. Yoda and M. Notomi, Generation and Annihilation of Topologically Protected Bound States in the Continuum and Circularly Polarized States by Symmetry Breaking, Phys. Rev. Lett. **125**, 053902 (2020).
[39] W. Chen, Y. Chen, and W. Liu, Line singularities and Hopf indices of electromagnetic multipoles, Laser Photonics Rev. **14**, 2000049 (2020).
[40] X. Yin, J. Jin, M. Soljačić, C. Peng, and B. Zhen, Observation of topologically enabled unidirectional guided resonances, Nature (London) **580**, 467 (2020).
[41] A. Abdrabou and Y. Y. Lu, Circularly polarized states and propagating bound states in the continuum in a periodic array of cylinders, Phys. Rev. A **103**, 043512 (2021).
[42] W. Ye, Y. Gao, and J. Liu, Singular Points of Polarizations in the Momentum Space of Photonic Crystal Slabs, Phys. Rev. Lett. **124**, 153904 (2020).
[43] C. Guo, M. Xiao, Y. Guo, L. Yuan, and S. Fan, Meron Spin Textures in Momentum Space, Phys. Rev. Lett. **124**, 106103 (2020).
[44] H. Zhou, C. Peng, Y. Yoon, C. Wei Hsu, K. A. Nelson, L. Fu, J. D. Joannopoulos, M. Soljačić, and B. Zhen, Observation of bulk Fermi arc and polarization half charge from paired exceptional points, Science **359**, 1009 (2018).
[45] W. Chen, Q. Yang, Y. Chen, and W. Liu, Evolution and global charge conservation for polarization singularities emerging from non-Hermitian degeneracies, Proc. Natl. Acad. Sci. U.S.A. **118**, e2019578118 (2021).
[46] M. V. Gorkunov, A. A. Antonov, and Y. S. Kivshar, Metasurfaces with Maximum Chirality Empowered by Bound States in the Continuum, Phys. Rev. Lett. **125**, 093903 (2020).
[47] W. Chen, Q. Yang, Y. Chen, and W. Liu, Extremize Optical Chiralities through Polarization Singularities, Phys. Rev. Lett. **126**, 253901 (2021).
[48] J. Wang, H. Li, Y. Ma, M. Zhao, W. Liu, B. Wang, S. Wu, X. Liu, L. Shi, T. Jiang, and J. Zi, Routing valley exciton emission of a WS_2 monolayer via delocalized Bloch modes of in-plane inversion-symmetry-broken photonic crystal slabs, Light **9**, 148 (2020).
[49] J. D. Joannopoulos, S. G. Johnson, J. N. Winn, and R. D. Meade, *Photonic Crystals: Molding the Flow of Light*, 2nd ed. (Princeton University Press, Princeton, NJ, 2008).
[50] H. S. Nguyen, F. Dubois, T. Deschamps, S. Cueff, A. Pardon, J.-L. Leclercq, C. Seassal, X. Letartre, and P. Viktorovitch, Symmetry Breaking in Photonic Crystals: On-Demand Dispersion from Flatband to Dirac Cones, Phys. Rev. Lett. **120**, 066102 (2018).
[51] S.-G. Lee, S.-H. Kim, and C.-S. Kee, Bound states in the continuum (BIC) accompanied by avoided crossings in leaky-mode photonic lattices, Nanophotonics **9**, 4373 (2020).
[52] See Supplemental Material at http://link.aps.org/supplemental/10.1103/PhysRevLett.127.176101 for (S1) the method of numerical simulations, (S2) the analysis with the temporal coupled-mode theory, (S3) the detail of the evolution of C points for downward radiation, (S4) the evolution of polarization singularities for other PCSs configurations, and (S5) the supplemental figures, which includes Refs. [53–56].
[53] C. W. Hsu, B. Zhen, M. Soljačić, and A. D. Stone, Polarization state of radiation from a photonic crystal slab, arXiv:1708.02197.
[54] H. Zhou, B. Zhen, C. W. Hsu, O. D. Miller, S. G. Johnson, J. D. Joannopoulos, and M. Soljačić, Perfect single-sided radiation and absorption without mirrors, Optica **3**, 1079 (2016).

[55] H. Friedrich and D. Wintgen, Interfering resonances and bound states in the continuum, Phys. Rev. A **32**, 3231 (1985).
[56] D. C. Marinica, A. G. Borisov, and S. V. Shabanov, Bound States in the Continuum in Photonics, Phys. Rev. Lett. **100**, 183902 (2008).
[57] S. Fan and J. D. Joannopoulos, Analysis of guided resonances in photonic crystal slabs, Phys. Rev. B **65**, 235112 (2002).
[58] S. Fan, W. Suh, and J. D. Joannopoulos, Temporal coupled-mode theory for the Fano resonance in optical resonators, J. Opt. Soc. Am. A **20**, 569 (2003).
[59] W. Suh, Z. Wang, and S. Fan, Temporal coupled-mode theory, and the presence of non-orthogonal modes in lossless multimode cavities, IEEE J. Quantum Electron. **40**, 1511 (2004).
[60] K. Koshelev, S. Lepeshov, M. Liu, A. Bogdanov, and Y. Kivshar, Asymmetric Metasurfaces with High-Q Resonances Governed by Bound States in the Continuum, Phys. Rev. Lett. **121**, 193903 (2018).
[61] Y. Guo, M. Xiao, and S. Fan, Topologically Protected Complete Polarization Conversion, Phys. Rev. Lett. **119**, 167401 (2017).
[62] Y. Guo, M. Xiao, Y. Zhou, and S. Fan, Arbitrary polarization conversion with a photonic crystal slab, Adv. Opt. Mater. **7**, 1801453 (2019).
[63] M. Dai, L. Ma, Y. Xu, M. Lu, X. Liu, and Y. Chen, Highly efficient and perfectly vertical chip-to-fiber dual-layer grating coupler, Opt. Express **23**, 1691 (2015).
[64] A. Michaels and E. Yablonovitch, Inverse design of near unity efficiency perfectly vertical grating couplers, Opt. Express **26**, 4766 (2018).
[65] Z. Chen and M. Segev, Highlighting photonics: looking into the next decade, eLight **1**, 2 (2021).